Original Research Article: full paper

(2022), «EUREKA: Physics and Engineering»
Number 4

THEORETICAL APPROACH FOR Fe(II/III) AND ITS CHLOROPHYLL-RELATED COMPLEXES AS SENSITIZERS IN DYE-SENSITIZED SOLAR CELLS

Mohamad Rodhi Faiz
Department of Mechanical Engineering[1]
Department of Electrical Engineering
State University of Malang
Jl. Semarang, Malang, Indonesia, 65145

Denny Widhiyanuriyawan ✉
Department of Mechanical Engineering[1]
denny_w@ub.ac.id

Eko Siswanto
Department of Mechanical Engineering[1]

Fazira Ilyana Abdul Razak
Department of Chemistry
Universiti Teknologi Malaysia
Johor Bahru, Johor, Malaysia, 81310

I Nyoman Gede Wardana
Department of Mechanical Engineering[1]

[1]Brawijaya University
Jl. Veteran, Malang, Indonesia, 65145

✉**Corresponding author**

Abstract

Dye is the key to the efficiency of harvesting solar energy in dye-sensitized solar cells (DSSCs). The dye performances such as light absorption, electron injection, and electron regeneration depend on the dye molecule structure. To predict it, one needs to compute the optimized molecule geometry, HOMO level, LUMO level, electron density distribution, energy gaps, and dipole moment in the ground and excited state. Chlorophyll-related chlorin and porphyrin, as well as their κ2O,O' complexes with Fe(II/III), were investigated with density functional theory (DFT) and time-dependent density functional theory (TD-DFT) computations using the B3LYP method and def2-TZVP basis set. NPA charges also were calculated to know the valence of the metal cations exactly. In general, the calculations show that the metal cations introduced occupied d orbitals with lower oxidation potentials than the chlorophyll ligand orbitals, which are responsible for the emergence of additional absorption bands. The states result in effective band broadening and the redshift of spectrum absorbance that is expected to improve DSSC performance.

Another requirement that has to be possessed is the ability of electron regeneration, electron injection, and dipole moment. The Fe(II) complex has fulfilled these requirements, but not the Fe(III) complex due to having a low electron injection capability. However, this work has shown that Fe(III) complex exhibits a non-innocence ligand. It results in trivalent to divalent state change, in the appearance of a ligand radical cation, an extra hole, and a broader absorption spectrum. It also can affect its other electronic properties, such as electron injection capability. Thus, it can be considered an attractive candidate for the sensitizer in DSSCs.

Keywords: Chlorophyll, DSSC, DFT, MLCT, d orbital, non-innocence ligand, ligand radical cation.

DOI: 10.21303/2461-4262.2022.002519

1. Introduction

As is well known, energy has become a world issue due to the limitations of fossil fuel reserves and the associated environmental problems. Many alternative energy sources are widely used as renewable substitutes for fossil fuels, such as wind power, hydroelectric energy, tidal energy, geothermal energy, biomass, nuclear energy, and solar energy. Among these, solar energy has emerged

as a particularly clean and promising option [1]. Solar energy can be converted into electrical energy need a solar cell device. Dye-sensitized solar cells (DSSCs), as the third generation solar cells [2, 3], have many advantages compared with silicon-based solar cells, such as low production costs, renewability of raw material, ease to manufacture, the good theoretical conversion efficiency of a photon to electron, modifiable color and transparency, and environmental friendliness [4].

DSSCs can absorb visible light due to the sensitizer, which is intermixed with a semiconductor with a relatively broad bandgap, a typical example of the latter being TiO_2. The sensitizer is essential in extending the absorption spectrum of TiO_2 from the ultraviolet region to the visible region, and the overlap of the resulting absorption spectrum with the solar spectrum determines the solar cell efficiency. Furthermore, electron injection, charge recombination, and other photoelectrochemical processes may influence the conversion efficiency from solar power to electric power [5].

Natural dyes as sensitizers are produced easily from the extraction of leaves, flowers, fruits, roots, tree barks, etc., and have many advantages, such as low cost, low toxicity, and environmental friendliness [6]. As an example, chlorophyll, which is typically obtained from leaf extraction, has two strong absorption peaks at 420 nm and 660 nm in the visible region and exhibits an open-circuit voltage (V_{oc}) of 0.585 mV, a short circuit current (J_{sc}) of 1.96 mA, a fill factor (FF) of 47 %, and conversion efficiency of 0.538 % in DSSC devices [7]. However, natural dyes also have disadvantages. They are easily degraded under heat, light, and acid conditions [8]. It can be improved by adding metal ions that can be introduced to give the corresponding metal complexes [9]. Most successful modifications of natural sensitizers involve ruthenium(II) polypyridyl-based compounds, which can improve the energy conversion efficiency of the DSSCs by up to 11 % [10]. But the synthesis is usually complicated and expensive, and the use of cheaper metal elements is desired [11–14].

One of them is metal iron, where many researchers have conducted experiments and succeeded in increasing the ability of dye absorption with the addition of metal iron in the organic dyes [15–18]. But theoretically, Fe(II/III) complex has an open-shell electronic structure and has low-lying non-emissive excited states, which result in not enough to facilitate efficient electron injection into the semiconductor. However, a research experimental provides motivation for choosing Fe(III) as a sensitizer due to its cheaper cost, better solubility, and relatively high quantum for producing sensitization on the nanocrystalline TiO_2 [19]. The theoretical study of this matter is still not clear and needs further investigation.

Therefore, in this work, let's study the Fe(II/III) complexes where the ligands contain chlorophyll-related chlorin and porphyrin as potential sensitizers for DSSCs. The study revealed how the metal ion Fe(II/III) affects the DSSC performances. Some parameters such as the electronic structure, absorption spectra, light-harvesting efficiency (LHE), the feasibility of electron injection, electron regeneration, and dipole moment were calculated by quantum chemical computation (DFT/TD-DFT), a popular approach for evaluating the performances of DSSCs [20].

2. Models and Computational Methods

2. 1. DSSC Parameters

Power conversion efficiency (η) of DSSCs depends on several factors, including short-circuit current density (J_{sc}), open-circuit photovoltage (V_{oc}), fill factor (FF), and the amount of solar power available to the solar cell (P_{in}), as in the following equation [21]:

$$\eta = \frac{J_{sc} V_{oc} FF}{P_{in}}, \tag{1}$$

where η can be improved by increasing J_{sc} and V_{oc}. The short-circuit current of a solar cell (J_{sc}) is the solar cell current when the voltage is zero and can be expressed as [22]:

$$J_{sc} = \int_{\lambda} LHE(\lambda)\Phi_{inject}\eta_{collect}d\lambda, \tag{2}$$

where $LHE(\lambda)$ is integrated against the light spectrum, including ultraviolet, visible, and near-infrared that the sensitizer can absorb, Φ_{inject} is the electron injection efficiency into the semiconductor,

and $\eta_{collect}$ is the charge collection efficiency for the semiconductor electrode. From the perspective of sensitizer design, the efficiency of light-harvesting (*LHE*) and the efficiency of electron injection (Φ_{inject}) uniquely determine J_{sc}. The efficiency of electron collection ($\eta_{collect}$) is constant because it only depends on the type of semiconductor, not on the kind of sensitizer [23]. The *LHE* is usually approximated by Beer's law [24] by substituting the absorbance with the oscillator strength *f*:

$$LHE(\lambda) = 1 - 10^{-f_{osc}}. \tag{3}$$

The larger the oscillator strength (f_{osc}) of the dye molecule, the better the sensitizer's ability to absorb light and, therefore, the *LHE*, which in turn leads to higher J_{sc} values [25]. Although the efficiency of electron injection (Φ_{inject}) is hard to compute quantitatively, it is positively correlated with the driving force of the electron injection into the semiconductor substrate from the excited state of dyes ($-\Delta G^{inject}$) via:

$$\Delta G^{inject} = E_{ox}^{dye^*} - E_{CB}^{SC}, \tag{4}$$

where $E_{ox}^{dye^*}$ represents the excited state oxidation potential of the dye and E_{CB}^{SC} represents the potential reduction energy of the semiconductor. The latter is calculated from the position of the conduction band (CB), which for TiO_2 is −4.0 eV. Let's note that by calculating ΔG^{inject} from energetic differences, there are implicitly dropping entropic contributions, which are presumably small. $E_{ox}^{dye^*}$ is calculated as [26]:

$$E_{ox}^{dye^*} = E_{ox}^{dye} - E_{0-0}, \tag{5}$$

where E_{ox}^{dye} represents the dye oxidation potential in the ground state and $E_{0\text{-}0}$ is the 0-0 transition energy, which is herein approximated by the vertical transition energy.

The open-circuit voltage can be calculated as [27]:

$$V_{oc} = \frac{E_{CB} + \Delta CB}{q} + \frac{kT}{q}\ln\left(\frac{n_c}{N_{CB}}\right) - \frac{E_{redox}}{q}, \tag{6}$$

where E_{CB} represents the conduction band edge energy of the semiconductor substrate, E_{redox} represents the redox potential of the electrolyte, k represents the Boltzmann constant (1.38×10^{-23} J/K), T represents the temperature, q represents the electron unit charge (1.6×10^{-19} C), N_{CB} is the conduction band (CB) accessible density, and n_c represents the number of conduction band electrons. ΔCB is the shift of E_{CB} when the surface of the semiconductor adsorbs the dye and can be computed as [28]:

$$\Delta CB = \frac{q\mu_{normal}\gamma}{\varepsilon_0\varepsilon}, \tag{7}$$

where q represents the electron unit charge, μ_{normal} represents the component of the dye molecule's dipole moment perpendicular to the surface of the semiconductor, γ represents the concentration of the dye, and ε and ε_0 represent the dielectric constant of the organic dye monolayer, and the vacuum permittivity, respectively.

2. 2. Computational Details

The computations were carried out on the Fe(II/III) complexes of chlorophyll-related porphyrin and chlorin, shown in **Fig. 1**, where the ion Fe(II/III) interacts with the carbonyl groups. The phytyl ester side chain of chlorophyll was replaced by hydrogen to reduce the computational cost [29].

All quantum chemical calculations have been performed with the ORCA 4.2.1 program package [30–32]. The optimization of geometry was carried out without symmetry constraints, and the def2-TZVP basis set was applied for all atoms [33, 34], together with the fully decontracted def2/J auxiliary basis set [35]. Vibrational frequencies were calculated under the harmonic approximation to confirm the nature of the stationary points. The hybrid B3LYP density functional was

used for the DFT and TD-DFT calculations [36, 37]. Solvent effects of the TD-DFT calculations were described by the CPCM model [38], with acetonitrile as the solvent to get the maximum light absorption ability. Otherwise, the geometry optimizations were solved in the gas phase without CPCM solvent model to get the minima energy. The RIJCOSX algorithm was used to speed up the calculations [39–41]. Tight criteria of SCF convergence and improved integration grids (Grid5, FinalGrid6) were used on all calculations. NPA charges analyses were computed with the JANPA program package [42, 43].

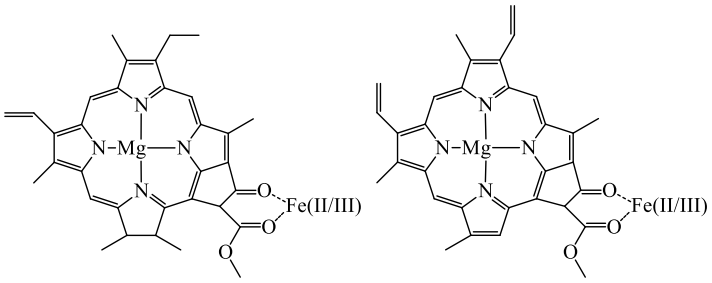

Fig. 1. Fe(II/III) complexes of chlorophyll-related: *a* – chlorin; *b* – porphyrin

3. Results and Discussion

3. 1. Coordination Environment of Metal Atoms

Fig. 1 schematically illustrates the Fe(II/III)-chlorophyll bonding without coordinating solvent. For adequate modeling of the systems, the iron centers must be explicitly solvated [44]. **Fig. 2** shows that four acetonitrile molecules were used to saturate the vacant coordination sites of Fe(II/III), as has been done in studies of chlorophyll-metal cation interactions [45], giving an octahedral molecular geometry, where the rest two coordination sites of Fe(II/III) are occupied by the ketone and ester carbonyl groups of the chlorophyll derivative [46]. **Table 1** shows the major geometric parameters of the metal complexes. For both the chlorin and the porphyrin derivatives, the average Mg-N distance, <Mg-N>, is slightly reduced by the presence of the Fe(II/III) cation. The coordination asymmetry, Δ(Mg-N), is defined as the difference between the longest and the shortest Mg-N bonds. With the presence of the Fe(II/III) cation, the asymmetry decreases for the chlorin derivative and increases for the porphyrin derivative. The <Fe-O> is the average distance of the two Fe-O bonds and is longer for Fe(III) than for Fe(II) in both the chlorin and porphyrin derivatives, which goes contrary to what is expected from electrostatics; moreover, the NPA charges of the Fe atoms of the Fe(II) and Fe(III) complexes are essentially the same, again are contrary to the formal oxidation states of Fe(II) and Fe(III). It is possible to see in the next section that these phenomena are indications of the ligand non-innocence of the Fe(III) complexes.

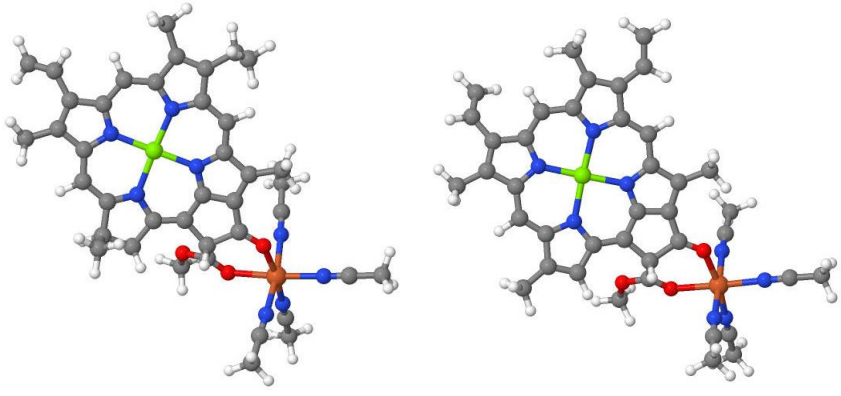

Fig. 2. Fe(II/III) complexes solvated by acetonitrile of chlorophyll-related: *a* – chlorin; *b* – porphyrin

Table 1

Major geometric parameters (distance in Å) of the Fe(II/III) complexes

–	Chlorin	Fe(II)-Chlorin	Fe(III)-Chlorin	Porphyrin	Fe(II)-Porphyrin	Fe(III)-Porphyrin
M-N(I)	2.136	2.128	2.124	2.085	2.084	2.089
M-N(II)	2.005	2.020	2.011	2.031	2.013	2.009
M-N(III)	2.022	2.015	2.010	2.063	2.060	2.058
M-N(IV)	2.060	2.053	2.048	2.016	2.012	2.015
<M-N>	2.056	2.054	2.048	2.049	2.042	2.042
Δ(M-N)	0.131	0.112	0.113	0.069	0.072	0.080
Fe-OCOMe	no Fe	2.224	2.223	no Fe	2.191	2.206
Fe-O	no Fe	2.009	2.120	no Fe	2.003	2.098
<Fe-O>	no Fe	2.117	2.172	no Fe	2.097	2.152
NPA charge of Fe	no Fe	1.48	1.5	no Fe	1.48	1.5

3. 2. Electronic Structures and Excited States

Tables 2, 3 show absorption wavelengths (λ_{max}), oscillator strengths (f_{osc}), light-harvesting efficiencies (*LHE*), vertical excitation energies ($E_{0\text{-}0}$), and dominant contributions to the excited states, calculated by TD-DFT. Upon inclusion of the Fe(II/III) cations, the absorption wavelengths undergo a bathochromic shift to beyond 600 nm, corresponding to vertical excitation energy of about 2 eV; for the Fe(III) complexes, the vertical excitation energies are further lowered to below 2 eV. The number of bright states increases as we go from the uncomplexed compound to the Fe(II) complex and then to the Fe(III) complex, consistent with the progressively increased involvement of the Fe atom in the electronic structures.

Table 2

Calculated f_{osc}, *LHE*, E_{0-0}, λ_{max}, and dominant contributions to the excited states for Fe(II/III)-chlorin. Only those excited states within the first 70 calculated roots with f_{osc}>0.05 are reported. Orbital transitions are only reported if their contributions are >10 %

Dyes	λ_{max} (nm)	$E_{0\text{-}0}$ (eV)	f_{osc}	*LHE* (%)	Dominant transition	Contribution %
Chlorin	558.3	2.221	0.318	51.92	H-1→L+1	21.49
					H→L	73.15
	375.2	3.305	0.478	66.73	H-1→L+1	28.40
					H→L+2	34.68
	318.5	3.893	0.924	88.09	H-1→L+2	43.65
					H→L+3	20.93
Fe(II)-Chlorin	611.3	2.028	0.068	14.49	H-1α→ Lα	34.70
					H-1β→Lβ	32.26
	559.7	2.215	0.431	62.93	Hα→Lα	32.28
					Hβ→Lβ	28.07
	397.8	3.117	0.161	30.98	Hα→L+2α	17.18
					Hβ→L+4β	35.59
	341.4	3.632	0.469	66.04	H-2α→L+1α	11.56
					H-3β→L+1β	15.10
Fe(III)-Chlorin	720.6	1.721	0.093	19.28	H-1α→Lα	17.11
					Hα→Lα	58.78
					H-5β→Lβ	10.34
	548.5	2.260	0.05	10.87	H-1α→Lα	9.40
					Hα→L+1α	12.81
					H-5β→Lβ	24.37
					Hβ→L+1β	32.95
	449.9	2.756	0.164	31.45	Hα→L+1α	15.28
					Hβ→L+2β	30.51
	352.3	3.519	0.110	22.38	H-6α→Lα	26.39
					H-12β→Lβ	39.81
	329.3	3.765	0.379	58.22	H-9α→Lα	37.94
					H-3β→L+2β	24.32

Table 3

Calculated f_{osc}, *LHE*, E_{0-0}, λ_{max}, and dominant contributions to the excited states for Fe(II/III)-porphyrin. Only those excited states within the first 70 calculated roots with f_{osc}>0.05 are reported. Orbital transitions are only reported if their contributions are >10 %

Dyes	λ_{max} (nm)	E_{0-0} (eV)	f_{osc}	*LHE* (%)	Dominant transition	Contribution %
Porphyrin	411.9	3.010	0.396	59.82	H-1→L+1	27.58
					H→L	14.14
					H→L+2	26.48
	412.1	3.008	0.094	19.46	H-2→L+1	86.60
	374.6	3.310	0.535	70.83	H-4→L	17.23
					H-1→L	13.30
					H-1→L+2	14.44
					H→L+1	18.39
					H→L+2	10.30
	335.3	3.698	0.728	81.29	H-5→L	19.62
					H-4→L+1	24.21
					H-1→L+2	11.23
					H→L+1	10.59
Fe(II)-Porphyrin	571.2	2.170	0.112	22.73	H-1α→Lα	34.01
					Hα→L+1α	15.62
					H-1β→Lβ	28.86
					Hβ→L+1β	17.52
	454.7	2.727	0.075	15.86	H-1α→L+2α	10.42
					Hβ→L+2β	16.79
					Hβ→L+4β	31.48
	443.2	2.798	0.083	17.43	H-1α→L+1α	13.20
					Hα→L+2α	54.03
					H-1β→L+1β	10.38
	410.5	3.020	0.158	30.50	H-2α→L+1α	38.10
					H-3β→L+1β	37.07
	401.3	3.089	0.066	14.10	H-3α→L+1α	30.92
					H-4β→L+1β	31.38
	383.3	3.234	0.363	56.65	H-3α→L+1α	14.07
					H-4β→L+1β	16.02
					H-1β→L+4β	17.18
Fe(III)-Porphyrin	634.2	1.955	0.051	11.08	H-1α→Lα	26.40
					H-1α→L+1α	10.00
					Hα→ Lα	25.95
					H-5β→Lβ	21.25
	559.7	2.215	0.05	10.87	H-1α→L+1α	32.77
					Hα→L+1α	20.02
					H-7β→Lβ	12.06
					Hβ→L+1β	20.20
	455.3	2.723	0.05	10.87	H-3α→L+1α	25.53
					H-9β→Lβ	18.16
	441.8	2.807	0.100	20.57	H-2α→L+1α	22.20
					H-1β→L+2β	37.17
	439.5	2.821	0.062	13.30	H-4α→Lα	21.23
					H-3α→L+1α	15.05
					H-4β→L+1β	10.60
	434.4	2.854	0.143	28.06	H-3α→L+1α	12.19
					H-10β→Lβ	14.15
	426.0	2.910	0.064	13.70	Hα→L+2α	31.62
					Hβ→L+3β	35.19
	418.7	2.961	0.088	18.34	H-3α→L+1α	12.70
					H-3β→L+2β	53.89
	385.1	3.220	0.170	32.39	H-1α→L+1α	10.00
					Hβ→L+5β	14.69

Fig. 3 show the frontier orbitals of chlorophyll-related porphyrin and chlorin and their Fe(II/III) complexes. Both the bidentate chlorophyll ligands and acetonitrile are weak field ligands, making all Fe cations high-spin. The Fe(II/III) complexes have lower HOMO-LUMO gaps than those of the uncomplexed compounds (**Fig. 4**; note that the HOMO-LUMO gap is defined as $min(E_{LUMO\alpha}-E_{HOMO\alpha}, E_{LUMO\beta}-E_{HOMO\beta}, E_{LUMO\alpha}-E_{HOMO\beta}, E_{LUMO\beta}-E_{HOMO\alpha})$). For the Fe(II) complexes, the reason for the reduced gap can be readily identified as the preferential mixing of the Fe d orbitals with the LUMOβ orbital of the ligands, which lowers the LUMOβ orbital by a larger extent than the HOMOα/HOMOβ orbitals and therefore reduces the HOMO-LUMO gap. The origin of the small gaps of the Fe(III) complexes, however, is different: the LUMOβs of the Fe(III) complexes have a different character from those of the free ligand and the Fe(II) complexes but have a similar shape with the HOMOα/HOMOβ orbitals of the latter. Let's, therefore, conclude that the highly oxidizing Fe(III) introduces a hole on the HOMOβ orbital of the ligand by oxidizing the ligand to its radical cation; as the gap between the HOMO and the HOMO-1 orbitals of the ligand is much smaller than the HOMO-LUMO gap, the ligand radical cation has a much smaller HOMO-LUMO gap than the ligand itself. The Fe(III) complex thus has an even smaller HOMO-LUMO gap than the Fe(II) complex, which was consistent with the previous research experiment [47]. After oxidizing the ligand, the Fe(III) center is reduced to the divalent state, which explains the abnormal trend of the Fe-O bond lengths and the Fe atomic charges as described in the previous section. For consistency, however, in the rest of the manuscript, it is possible to still refer to these complexes as the Fe(III) complexes, despite that the Fe centers are not actually trivalent.

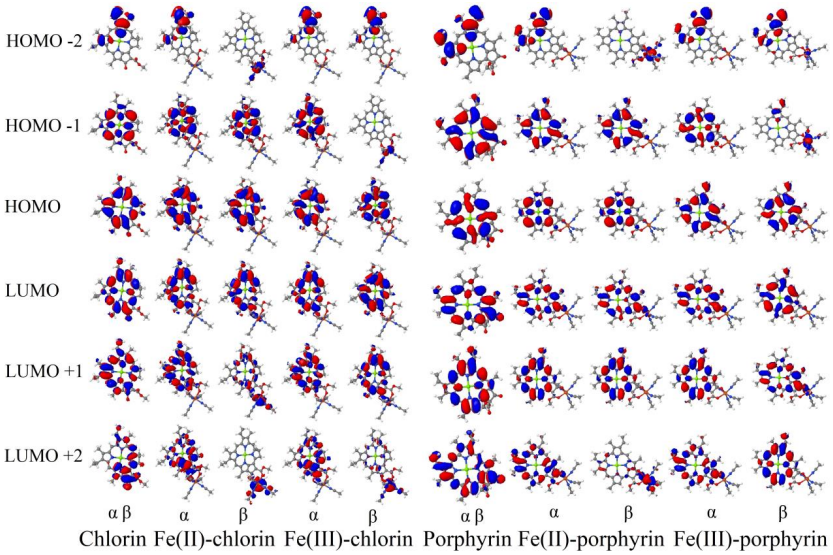

Fig. 3. Frontier orbitals of chlorophyll-related and its complexes

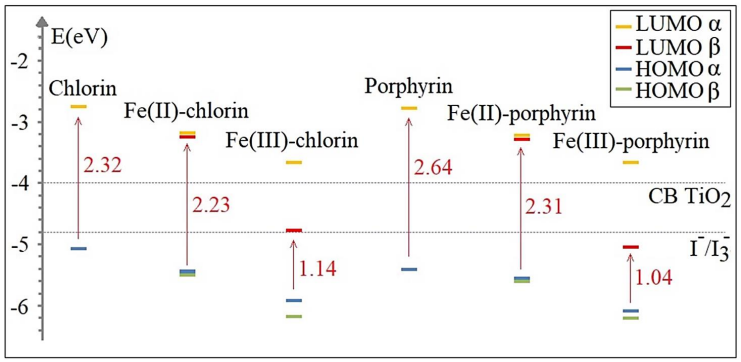

Fig. 4. Energy levels of chlorophyll-related and its complexes, conduction band of TiO_2, and redox potential of the I^-/I_3^- electrolyte

As for the compositions of excited states discussion, it was shown that the frontier orbitals of the complexes comprise both metal d orbitals and ligand π orbitals. This enables the compounds to undergo charge transfer from metal to ligand (MLCT), ligand to metal charge transfer (LMCT), ligand field d-d transitions, and ligand to ligand transitions [48, 49]. **Fig. 3** shows that the excitations of the chlorophyll are dominated by the $\pi \rightarrow \pi^*$ character, while for the Fe(II/III) complex, a mixture of both $d \rightarrow \pi^*$ and $\pi \rightarrow \pi^*$ transitions are seen. The first excited state of Fe(II)-chlorin at $E_{0\text{-}0} = 0.27$ eV with $f_{osc} = 0.00001$ is a mixture of MLCT and metal d-d transitions and is dominated by the transition from HOMO-2β to LUMO+2β with 16 % contribution and HOMO-2β to LUMO+1β with 57 % contribution. A similar observation can be made for the Fe(II)-porphyrin, where the first excited state occurs at $E_{0\text{-}0} = 0.25$ eV with $f_{osc} = 0.00003$ and is dominated by the d-d transition from HOMO-2β to LUMO+2β with 75 % contribution. Likewise, the first excited states of Fe(III)-chlorin and Fe(III)-porphyrin have $E_{0\text{-}0} = 0.21$ eV and 0.19 eV, respectively, both with the oscillator strength $f_{osc} = 0.00007$, and are dominated by ligand field transitions from HOMO-1β to LUMO+2β (71 %) and HOMO-1β to LUMO+3β (61 %), respectively. The aforementioned excited states were, however, not listed in **Tables 2, 3** because their oscillator strengths are smaller than 0.05. In contrast to MLCT transitions, LMCT transitions generally do not strongly dominate any excited state. The bright states of the Fe(II/III) complexes all possess predominantly $\pi \rightarrow \pi^*$ character, but small admixtures of LMCT contributions are sometimes present, which in part explains the increased number of bright states of the Fe(II/III) complexes compared to the free ligands.

3. 3. Optical Characteristics

Fig. 5, 6 show the spectra of chlorophyll-related chlorin and porphyrin, as well as their Fe(II/III) complexes.

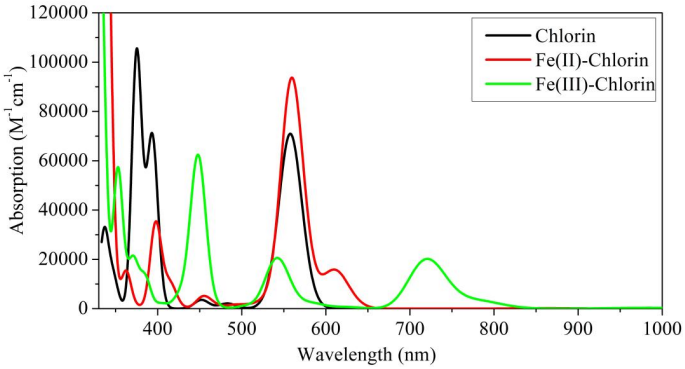

Fig. 5. Absorption spectra of chlorin and Fe(II/III)-chlorin

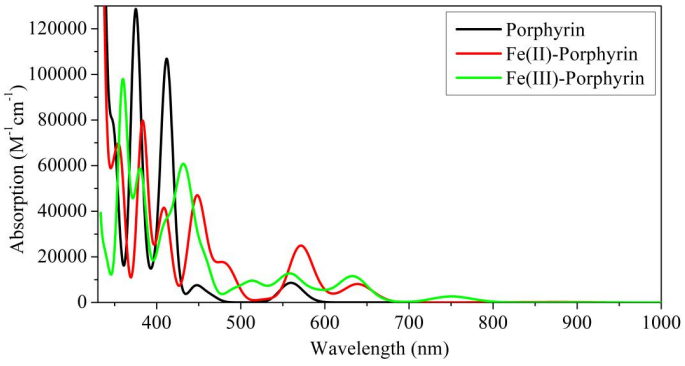

Fig. 6. Absorption spectra of porphyrin and Fe(II/III)-porphyrin

Consistent with **Tables 2, 3**, the Fe complexes feature more absorption peaks, which is especially true for the Fe(III) complexes. Thus, the introduction of Fe(II/III) greatly broadens the

absorption wavelength range of the dyes, which is beneficial for the efficient utilization of solar energy. Moreover, the Fe(II/III) ions induce a bathochromic shift of the lowest absorption bands of the compounds. The main reason for the improved performances is different for Fe(II) and Fe(III). For the Fe(II) complexes, the gain of performance is mainly attributed to MLCT transitions. The Fe(III) complex was, however, found to possess a Fe(II)-(ligand radical cation) electronic structure, and the additional excitations brought about by the extra hole on the ligand are the main reason for the performance gain. The additional bands give the metal complexes a much wider absorption window in the visible region than the uncomplexed dyes, making the metal complexes more efficient absorbers of sunlight and, therefore, possibly more efficient sensitizers for DSSCs due to an increase in short-circuit current of the solar cell (J_{sc}) as shown in (2).

3. 4. Properties of Redox and Charge Transfer to TiO_2

The HOMO and LUMO levels, ΔG^{inject}, and dipole moment are listed in **Table 4** to assess the redox properties of the dyes. The LUMO energy level must be higher than the CB of TiO_2 by more than 0.2 eV to have large enough electron injection efficiencies (Φ_{inject}) [50, 51], as follows from equation (4). **Table 4** shows that the ΔG^{inject} of all dyes satisfies this criterion, except for the Fe(III) complexes, where the LUMOβ energy level is lower than the CB of TiO_2, but LUMOα was instead higher than CB TiO_2. Nevertheless, as the first bright states of both Fe(III) complexes have more contributions from LUMOα than from LUMOβ, electron injection may still be possible if the electron injection is fast enough to compete with the decay of the bright states. Besides, the HOMO energy levels of all the dyes are lower than the redox potential of the I^-/I_3^- electrolyte redox pair (−4.8 eV), which means that the oxidized dye can be effectively regenerated by the iodide [20, 52]. The fact that both HOMO and LUMO levels are lowered appreciably due to the presence of the metal cation is consistent with K. Saito's model [53].

The dipole moment and the charge transfer to TiO_2 were computed using the dye-$Ti(OH)_4$ binding model [54, 55]. The $Ti(OH)_4$ bond to the carbonyl of the phytyl groups with the monodentate bond. The dipole moment affects the magnitude of open-circuit solar cell voltage (V_{oc}) as in equations (6), (7). It can be seen that the highest dipole moment is the Fe(II) complex. **Fig. 7** shows the electron density distribution of the HOMO-LUMO states.

Table 4

HOMO levels (eV), LUMO levels (eV), HOMO-LUMO gaps (eV), ΔG^{inject} (eV), and dipole moment (Debye) of chlorophyll-related chlorin and porphyrin and their Fe(II/III) complexes

No.	Dyes	HOMO		LUMO		HOMO-LUMO Gap	ΔG^{inject}		Dipole Moment
		α	β	α	β		α	β	
1	Chlorin	–5.07	–5.07	–2.76	–2.76	2.32	1.24	1.24	8.8
2	Fe(II)-Chlorin	–5.49	–5.50	–3.18	–3.26	2.23	0.82	0.74	21.5
3	Fe(III)-Chlorin	–5.92	–6.19	–3.66	–4.78	1.14	0.34	–0.78	13.2
4	Porphyrin	–5.41	–5.41	–2.78	–2.78	2.64	1.22	1.22	8.5
5	Fe(II)-Porphyrin	–5.61	–5.61	–3.22	–3.29	2.31	0.78	0.71	22.5
6	Fe(III)-Porphyrin	–6.10	–6.23	–3.68	–5.06	1.04	0.32	–1.06	13.1

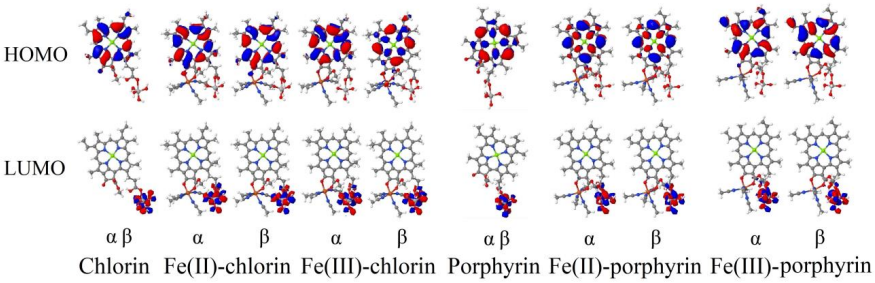

Fig. 7. HOMO-LUMO electron density distributions of dye-TiO_2 bonds

The distribution indicates there is a charge transfer from the dye to TiO_2 totally. The distribution occurs in the visible region for the chlorin, porphyrin, and F(II) complexes in all states but only in the UV region for the Fe(III) complexes. This strengthens the statement above that the electron injection capability of the Fe(III) complex is weak.

3. 5. Limitations and direction for the development of the study

Due to the abundant reserve and low cost of the iron synthesis, many researchers are interested in this material experiment. A statement stating that the Fe(III) ion has an open shell with low injectability was declined by a research experiment. The given facts showed that the Fe(III) ion could improve the DSSCs performance. Furthermore, this study provides several findings on the phenomena: non-innocence ligand, ligand radical cation, valence change, extra hole, and sufficient LUMOα energy level. These indicate that the Fe(III) complex can be considered an applicant for DSSC sensitizer. However, this study has limitations. It does not examine strategies to optimize these phenomena. These limitations emerge topics to be addressed in further development, including the influence of the solvents, type of ligands, and possibly acid-base treatments.

4. Conclusions

The theoretical investigation of Fe(II)-chlorophyll-related chlorin and porphyrin by DFT and TD-DFT reveal that the dyes are potential candidates for the sensitizer in DSSCs with UV-Vis absorption maxima well within the visible region. HOMO/LUMO levels are also compatible with the redox potential of I^-/I_3^- and the CB of TiO_2, respectively. The presence of the Fe(II) cation shifts the lowest energy absorption to longer wavelengths owing to the participation of the metal d orbitals in the excitations, which are mainly attributed to MLCT transitions. Furthermore, Fe(III) complex dyes are unsuitable for DSSC because of their low electron injection ability. However, the work found a non-innocence ligand with the ligand radical cation that can convert trivalent to divalent states. It leads to having an extra hole and a broader absorption spectrum than Fe(II) complex. Many research experiments have succeeded in increasing the performance of DSSC by adding Fe(III) ions. It could be due to the non-innocence ligand during the synthesis that affects the type of bond as well as the ability of the electron injection. Thus, this manuscript provides an opportunity for future work on Fe(III) complexes in order to understand the mechanism and reasons behind the given facts.

Acknowledgments

We gratefully acknowledge the support of DRPM RISTEK DIKTI with the grant contract number: 3.4.8/UN32.14/LT/2017 or 21.8.23/UN32.14/LT/2017. We are also grateful for technical support from Conversion Energy Laboratory at the Department of Electrical Engineering, Universitas Negeri Malang, and the Department of Mechanical Engineering, Brawijaya University. Also, special thanks for the contribution of Mr. Zikuan Wang from Beijing National Laboratory for Molecular Sciences, College of Chemistry and Molecular Engineering, Peking University, Beijing, China.

References

[1] Lewis, N. S., Crabtree, G., Nozik, A. J., Wasielewski, M. R., Alivisatos, P., Kung, H. et. al. (2005). Basic Research Needs for Solar Energy Utilization. Report of the Basic Energy Sciences Workshop on Solar Energy Utilization. U.S. Department of Energy Office of Scientific and Technical Information. doi: https://doi.org/10.2172/899136

[2] Wu, C., Wang, K., Batmunkh, M., Bati, A. S. R., Yang, D., Jiang, Y. et. al. (2020). Multifunctional nanostructured materials for next generation photovoltaics. Nano Energy, 70, 104480. doi: https://doi.org/10.1016/j.nanoen.2020.104480

[3] Babar, F., Mehmood, U., Asghar, H., Mehdi, M. H., Khan, A. U. H., Khalid, H. et. al. (2020). Nanostructured photoanode materials and their deposition methods for efficient and economical third generation dye-sensitized solar cells: A comprehensive review. Renewable and Sustainable Energy Reviews, 129, 109919. doi: https://doi.org/10.1016/j.rser.2020.109919

[4] O'Regan, B., Grätzel, M. (1991). A low-cost, high-efficiency solar cell based on dye-sensitized colloidal TiO2 films. Nature, 353 (6346), 737–740. doi: https://doi.org/10.1038/353737a0

[5] Odobel, F., Pellegrin, Y., Gibson, E. A., Hagfeldt, A., Smeigh, A. L., Hammarström, L. (2012). Recent advances and future directions to optimize the performances of p-type dye-sensitized solar cells. Coordination Chemistry Reviews, 256 (21-22), 2414–2423. doi: https://doi.org/10.1016/j.ccr.2012.04.017

[6] Al-Ghamdi, A. A., Gupta, R. K., Kahol, P. K., Wageh, S., Al-Turki, Y. A., El Shirbeeny, W., Yakuphanoglu, F. (2014). Improved solar efficiency by introducing graphene oxide in purple cabbage dye sensitized TiO2 based solar cell. Solid State Communications, 183, 56–59. doi: https://doi.org/10.1016/j.ssc.2013.12.021

[7] Syafinar, R., Gomesh, N., Irwanto, M., Fareq, M., Irwan, Y. M. (2015). Chlorophyll Pigments as Nature Based Dye for Dye-Sensitized Solar Cell (DSSC). Energy Procedia, 79, 896–902. doi: https://doi.org/10.1016/j.egypro.2015.11.584

[8] Tamiaki, H., Tsuji, K., Kuno, M., Kimura, Y., Watanabe, H., Miyatake, T. (2016). Synthesis of chlorophyll- a derivatives methylated in the 3-vinyl group and their intrinsic site energy. Bioorganic & Medicinal Chemistry Letters, 26 (13), 3034–3037. doi: https://doi.org/10.1016/j.bmcl.2016.05.008

[9] Refat, M. S. (2013). Synthesis and characterization of ligational behavior of curcumin drug towards some transition metal ions: Chelation effect on their thermal stability and biological activity. Spectrochimica Acta Part A: Molecular and Biomolecular Spectroscopy, 105, 326–337. doi: https://doi.org/10.1016/j.saa.2012.12.041

[10] Shalini, S., Balasundara prabhu, R., Prasanna, S., Mallick, T. K., Senthilarasu, S. (2015). Review on natural dye sensitized solar cells: Operation, materials and methods. Renewable and Sustainable Energy Reviews, 51, 1306–1325. doi: https://doi.org/10.1016/j.rser.2015.07.052

[11] Arkan, F., Izadyar, M. (2017). The investigation of the central metal effects on the porphyrin-based DSSCs performance; molecular approach. Materials Chemistry and Physics, 196, 142–152. doi: https://doi.org/10.1016/j.matchemphys.2017.04.054

[12] Arkan, F., Izadyar, M., Nakhaeipour, A. (2016). The role of the electronic structure and solvent in the dye-sensitized solar cells based on Zn-porphyrins: Theoretical study. Energy, 114, 559–567. doi: https://doi.org/10.1016/j.energy.2016.08.027

[13] Özkan, G., Ersus Bilek, S. (2015). Enzyme-assisted extraction of stabilized chlorophyll from spinach. Food Chemistry, 176, 152–157. doi: https://doi.org/10.1016/j.foodchem.2014.12.059

[14] Han, J., Wang, Y., Ma, J., Wu, Y., Hu, Y., Ni, L., Li, Y. (2013). Simultaneous aqueous two-phase extraction and saponification reaction of chlorophyll from silkworm excrement. Separation and Purification Technology, 115, 51–56. doi: https://doi.org/10.1016/j.seppur.2013.04.047

[15] Çakar, S., Özacar, M. (2019). The pH dependent tannic acid and Fe-tannic acid complex dye for dye sensitized solar cell applications. Journal of Photochemistry and Photobiology A: Chemistry, 371, 282–291. doi: https://doi.org/10.1016/j.jphotochem.2018.11.030

[16] Çakar, S. (2019). 1,10 phenanthroline 5,6 diol metal complex (Cu, Fe) sensitized solar cells: A cocktail dye effect. Journal of Power Sources, 435, 226825. doi: https://doi.org/10.1016/j.jpowsour.2019.226825

[17] Wang, D., Sun, Y., Shang, Q., Wang, X., Guo, T., Guan, H., Lu, Q. (2017). Effects of the conjugated structure of Fe-bipyridyl complexes on photoinduced electron transfer in TiO_2 photocatalytic systems. Journal of Catalysis, 356, 32–42. doi: https://doi.org/10.1016/j.jcat.2017.09.009

[18] Ferreira, H., von Eschwege, K. G., Conradie, J. (2016). Electronic properties of Fe charge transfer complexes – A combined experimental and theoretical approach. Electrochimica Acta, 216, 339–346. doi: https://doi.org/10.1016/j.electacta.2016.09.034

[19] Setyawati, H., Darmokoesoemo, H., Ningtyas, A. T. A., Kadmi, Y., Elmsellem, H., Kusuma, H. S. (2017). Effect of metal ion Fe(III) on the performance of chlorophyll as photosensitizers on dye sensitized solar cell. Results in Physics, 7, 2907–2918. doi: https://doi.org/10.1016/j.rinp.2017.08.009

[20] Lu, Y.-H., Liu, R.-R., Zhu, K.-L., Song, Y.-L., Geng, Z.-Y. (2016). Theoretical study on the application of double-donor branched organic dyes in dye-sensitized solar cells. Materials Chemistry and Physics, 181, 284–294. doi: https://doi.org/10.1016/j.matchemphys.2016.06.060

[21] Ren, X., Jiang, S., Cha, M., Zhou, G., Wang, Z.-S. (2012). Thiophene-Bridged Double D-π-A Dye for Efficient Dye-Sensitized Solar Cell. Chemistry of Materials, 24 (17), 3493–3499. doi: https://doi.org/10.1021/cm302250y

[22] Preat, J., Jacquemin, D., Perpète, E. A. (2010). Towards new efficient dye-sensitised solar cells. Energy & Environmental Science, 3 (7), 891. doi: https://doi.org/10.1039/c000474j

[23] Zhang, J., Li, H.-B., Sun, S.-L., Geng, Y., Wu, Y., Su, Z.-M. (2012). Density functional theory characterization and design of high-performance diarylamine-fluorenedyes with different π spacers for dye-sensitized solar cells. J. Mater. Chem., 22 (2), 568–576. doi: https://doi.org/10.1039/c1jm13028e

[24] Fan, W., Tan, D., Deng, W.-Q. (2012). Acene-Modified Triphenylamine Dyes for Dye-Sensitized Solar Cells: A Computational Study. ChemPhysChem, 13 (8), 2051–2060. doi: https://doi.org/10.1002/cphc.201200064

[25] Preat, J., Jacquemin, D., Michaux, C., Perpète, E. A. (2010). Improvement of the efficiency of thiophene-bridged compounds for dye-sensitized solar cells. Chemical Physics, 376 (1-3), 56–68. doi: https://doi.org/10.1016/j.chemphys.2010.08.001

[26] Preat, J., Michaux, C., Jacquemin, D., Perpète, E. A. (2009). Enhanced Efficiency of Organic Dye-Sensitized Solar Cells: Triphenylamine Derivatives. The Journal of Physical Chemistry C, 113 (38), 16821–16833. doi: https://doi.org/10.1021/jp904946a

[27] Marinado, T., Nonomura, K., Nissfolk, J., Karlsson, M. K., Hagberg, D. P., Sun, L. et. al. (2009). How the Nature of Triphenylamine-Polyene Dyes in Dye-Sensitized Solar Cells Affects the Open-Circuit Voltage and Electron Lifetimes. Langmuir, 26 (4), 2592–2598. doi: https://doi.org/10.1021/la902897z

[28] Lu, J., Meng, Q., Zhang, L., Liu, Y., Liu, W., Zhang, X. (2015). Single crystal structure, self-assembled nano-structure and semiconductor properties of a sandwich-type mixed (phthalocyaninato)(porphyrinato) europium triple-decker complex. Dyes and Pigments, 115, 1–6. doi: https://doi.org/10.1016/j.dyepig.2014.12.005

[29] Bechaieb, R., Ben Akacha, A., Gérard, H. (2016). Quantum chemistry insight into Mg-substitution in chlorophyll by toxic heavy metals: Cd, Hg and Pb. Chemical Physics Letters, 663, 27–32. doi: https://doi.org/10.1016/j.cplett.2016.09.053

[30] Neese, F. (2011). The ORCA program system. WIREs Computational Molecular Science, 2 (1), 73–78. doi: https://doi.org/10.1002/wcms.81

[31] Neese, F. (2017). Software update: the ORCA program system, version 4.0. WIREs Computational Molecular Science, 8 (1). doi: https://doi.org/10.1002/wcms.1327

[32] Neese, F., Wennmohs, F., Becker, U., Riplinger, C. (2020). The ORCA quantum chemistry program package. The Journal of Chemical Physics, 152 (22), 224108. doi: https://doi.org/10.1063/5.0004608

[33] Weigend, F., Ahlrichs, R. (2005). Balanced basis sets of split valence, triple zeta valence and quadruple zeta valence quality for H to Rn: Design and assessment of accuracy. Physical Chemistry Chemical Physics, 7 (18), 3297. doi: https://doi.org/10.1039/b508541a

[34] Schäfer, A., Horn, H., Ahlrichs, R. (1992). Fully optimized contracted Gaussian basis sets for atoms Li to Kr. The Journal of Chemical Physics, 97 (4), 2571–2577. doi: https://doi.org/10.1063/1.463096

[35] Weigend, F. (2006). Accurate Coulomb-fitting basis sets for H to Rn. Physical Chemistry Chemical Physics, 8 (9), 1057. doi: https://doi.org/10.1039/b515623h

[36] Becke, A. D. (1993). Density-functional thermochemistry. III. The role of exact exchange. The Journal of Chemical Physics, 98 (7), 5648–5652. doi: https://doi.org/10.1063/1.464913

[37] Lee, C., Yang, W., Parr, R. G. (1988). Development of the Colle-Salvetti correlation-energy formula into a functional of the electron density. Physical Review B, 37 (2), 785–789. doi: https://doi.org/10.1103/physrevb.37.785

[38] Barone, V., Cossi, M. (1998). Quantum Calculation of Molecular Energies and Energy Gradients in Solution by a Conductor Solvent Model. The Journal of Physical Chemistry A, 102 (11), 1995–2001. doi: https://doi.org/10.1021/jp9716997

[39] Andrae, D., Haeussermann, U., Dolg, M., Stoll, H., Preuss, H. (1990). Energy-adjustedab initio pseudopotentials for the second and third row transition elements. Theoretica Chimica Acta, 77 (2), 123–141. doi: https://doi.org/10.1007/bf01114537

[40] Neese, F. (2003). An improvement of the resolution of the identity approximation for the formation of the Coulomb matrix. Journal of Computational Chemistry, 24 (14), 1740–1747. doi: https://doi.org/10.1002/jcc.10318

[41] Neese, F., Wennmohs, F., Hansen, A., Becker, U. (2009). Efficient, approximate and parallel Hartree-Fock and hybrid DFT calculations. A «chain-of-spheres» algorithm for the Hartree-Fock exchange. Chemical Physics, 356 (1-3), 98–109. doi: https://doi.org/10.1016/j.chemphys.2008.10.036

[42] Nikolaienko, T. Y., Bulavin, L. A., Hovorun, D. M. (2014). JANPA: An open source cross-platform implementation of the Natural Population Analysis on the Java platform. Computational and Theoretical Chemistry, 1050, 15–22. doi: https://doi.org/10.1016/j.comptc.2014.10.002

[43] Nikolaienko, T. Y., Bulavin, L. A. (2018). Localized orbitals for optimal decomposition of molecular properties. International Journal of Quantum Chemistry, 119 (3), e25798. doi: https://doi.org/10.1002/qua.25798

[44] Jaramillo, P., Coutinho, K., Cabral, B. J. C., Canuto, S. (2012). Ionization of chlorophyll-c2 in liquid methanol. Chemical Physics Letters, 546, 67–73. doi: https://doi.org/10.1016/j.cplett.2012.07.040

[45] Kunieda, M., Tamiaki, H. (2008). Synthesis of Zinc 3-Hydroxymethyl-porphyrins Possessing Carbonyl Groups at the 13- and/or 15-Positions for Models of Self-Aggregative Chlorophylls in Green Photosynthetic Bacteria. The Journal of Organic Chemistry, 73 (19), 7686–7694. doi: https://doi.org/10.1021/jo8014402

[46] Bechaieb, R., Fredj, A. B., Akacha, A. B., Gérard, H. (2016). Interactions of copper(II) and zinc(II) with chlorophyll: insights from density functional theory studies. New Journal of Chemistry, 40 (5), 4543–4549. doi: https://doi.org/10.1039/c5nj03244j

[47] Wu, Z., Xu, Z., Tan, H., Li, X., Yan, J., Dong, C., Zhang, L. (2019). Two novel rhodamine-based fluorescent probes for the rapid and sensitive detection of Fe^{3+}: Experimental and DFT calculations. Spectrochimica Acta Part A: Molecular and Biomolecular Spectroscopy, 213, 167–175. doi: https://doi.org/10.1016/j.saa.2019.01.032

[48] Chen, H., Wang, J., Zhao, F., Wang, Y., He, H., Xia, H. (2019). Synthesis, spectroscopic and DFT studies of copper(I) complexes inserting the electron-donating groups into pyridine-imidazole ligands vis an acetylide linker. Inorganica Chimica Acta, 498, 119155. doi: https://doi.org/10.1016/j.ica.2019.119155

[49] Erden, I., Hatipoglu, A., Cebeci, C., Aydogdu, S. (2020). Synthesis of D-π-A type 4,5-diazafluorene ligands and Ru (II) complexes and theoretical approaches for dye-sensitive solar cell applications. Journal of Molecular Structure, 1201, 127202. doi: https://doi.org/10.1016/j.molstruc.2019.127202

[50] Wang, C., Li, J., Cai, S., Ning, Z., Zhao, D., Zhang, Q., Su, J.-H. (2012). Performance improvement of dye-sensitizing solar cell by semi-rigid triarylamine-based donors. Dyes and Pigments, 94 (1), 40–48. doi: https://doi.org/10.1016/j.dyepig.2011.11.002

[51] Li, R., Lv, X., Shi, D., Zhou, D., Cheng, Y., Zhang, G., Wang, P. (2009). Dye-Sensitized Solar Cells Based on Organic Sensitizers with Different Conjugated Linkers: Furan, Bifuran, Thiophene, Bithiophene, Selenophene, and Biselenophene. The Journal of Physical Chemistry C, 113 (17), 7469–7479. doi: https://doi.org/10.1021/jp900972v

[52] El Mahdy, A. M., Halim, S. A., Taha, H. O. (2018). DFT and TD-DFT calculations of metallotetraphenylporphyrin and metallotetraphenylporphyrin fullerene complexes as potential dye sensitizers for solar cells. Journal of Molecular Structure, 1160, 415–427. doi: https://doi.org/10.1016/j.molstruc.2018.02.041

[53] Saito, K., Mitsuhashi, K., Ishikita, H. (2020). Dependence of the chlorophyll wavelength on the orientation of a charged group: Why does the accessory chlorophyll have a low site energy in photosystem II? Journal of Photochemistry and Photobiology A: Chemistry, 402, 112799. doi: https://doi.org/10.1016/j.jphotochem.2020.112799

[54] Nogueira, A. E., Ribeiro, L. S., Gorup, L. F., Silva, G. T. S. T., Silva, F. F. B., Ribeiro, C., Camargo, E. R. (2018). New Approach of the Oxidant Peroxo Method (OPM) Route to Obtain $Ti(OH)_4$ Nanoparticles with High Photocatalytic Activity under Visible Radiation. International Journal of Photoenergy, 2018, 1–10. doi: https://doi.org/10.1155/2018/6098302

[55] AL-Temimei, F. A., Omran Alkhayatt, A. H. (2020). A DFT/TD-DFT investigation on the efficiency of new dyes based on ethyl red dye as a dye-sensitized solar cell light-absorbing material. Optik, 208, 163920. doi: https://doi.org/10.1016/j.ijleo.2019.163920

Received date 07.12.2021
Accepted date 20.07.2022
Published date 30.07.2022

How to cite: *Faiz, M. R., Widhiyanuriyawan, D., Siswanto, E., Razak, F. I. A., Wardana, I. N. G. (2022). Theoretical approach for Fe(II/III) and its chlorophyll-related complexes as sensitizers in dye-sensitized solar cells. EUREKA: Physics and Engineering, 4, 3–15. https://doi.org/10.21303/2461-4262.2022.002519*